Volume : 4 | Issue : 10 | October 2015 • ISSN No 2277 - 8179

Research Paper

Cefalexin: Molecular Structure,Vibrational Spectroscopy,Natural Bond Orbital Analysis and HOMO,LUMO Studies

Physics

KEYWORDS : CFX, FT-IR, FT-Raman, NBO, MEP

P.S.Ganeshvar	Department of Physics, Karpagam University, Eachanari, Coimbatore 641021, TN, India
S.Gunasekaran	Research and Development St.Peter's Institute of Higher Education and Research, St.Peter's University, Avadi, Chennai -600 054, TN, India
T.Gnanasambandan	Department of Physics, Pallavan College of Engineering, Kanchipuram 631 502, TN, India
K.Viswanathan	Department of Physics, Karpagam University, Eachanari, Coimbatore 641021, TN, India

ABSTRACT

The spectroscopic properties of the Cefalexin (CFX) were examined by FT-IR, FT-Raman and UV-Vis techniques. FT-IR and FT-Raman spectra in solid state were observed in the region 4000-400cm-1 and 3500-100cm-1 respectively. The UV-Vis absorption spectrum of the compound that dissolved in water was recorded in the range of 200-400nm. The structural and spectroscopic data of the molecule in the ground state were calculated by using density functional theory (DFT) employing B3LYP method with 6-31G(d,p) basis set. Complete vibrational assignments aided by the theoretical harmonic frequencies calculated were compared with experimental FT-IR and FT-Raman spectra. The observed and the calculated frequencies are found to be in good agreement. The calculated HOMO and LUMO energies show that charge transfer occurs within the molecule.

1. Introduction

Cefalexin (CFX) compound belongs to the Cephalosporins. These are compounds containing a 1,2-thiazine fused to a 2-azetidinone for a oxo-5-thia-1-azabicyclo[4,2,0] oct-2-ene-2-carboxylic acid moiety or a derivative thereof. The title compound is a first generation cephalosporin antibiotic. It is one of the most widely prescribed antibiotics, often used for the treatment of superficial infections that result as complications of minor wounds or lacerations. It is effective against most gram-positive bacteria.

The CFX and its derivatives were studied by several authors. Madaras-kelly et.al. conclude that CFX remains the preferred antibiotic treatment for uncomplicated cellulitis. Patients with non-β-lactam regimens, primarily tetracycline and macrolides, had more side effects and did less well than CFX patients [1]. In the hospital, oral antibiotic therapy decreases length of stay, eliminates phlebitis / IV line infections, and is less expensive than parenteral therapy [2,3]. Golightly et al. issue can be circumvented by using Surface Enhanced Raman Scattering (SERS). The use of SERS requires the presence of a roughened surface made of metals or colloids [4,5]. In recent decades, different physical forms of solid active pharmaceutical ingredients (APIs) have evolved from a mere scientific curiosity to an issue that must be addressed for every dosage form [6-8]. In comparison, the Raman spectroscopic technique utilizes a monochromatic light source (e.g. a laser) focusing on a sample and analyzing the resulting scattered light [9].

Literature survey reveals, to the best of the present research student's knowledge, that DFT frequency calculations of the title compound CFX have not been reported so far. Therefore, the present investigation has been undertaken to study the molecular structure, geometrical parameters, vibrational wavenumbers, modes of vibrations and the Natural Bond Orbital (NBO) analysis which explain the most important orbital interactions in order to classify general structural features. CFX molecule can show large first order hyperpolarizabilities (β) related to an electronic intra-molecular charge transfer excitation between the ground and excited states calculation were performed by using DFT-B3LYP methods with 6-31G(d,p) basis set. By analyzing the density of states, the molecular orbital compositions and their contributions to the chemical bonding were studied. The study of HOMO, LUMO analysis were used to elucidate information regarding charge transfer within the molecule. Moreover, the Mulliken population analyses of the title compound were calculated and the calculated results reported. The experimental and theoretical results supported each other, and the calculations are valuable for providing a reliable insight into the vibrational spectra and molecular properties.

2. Experimental Details

The compound under investigation namely, CFX was purchased from APEX chemicals, Chennai which was of spectroscopic grade and hence, used for recording the spectra as such without any further purification. The FT-IR spectra of the compounds were recorded in Bruker IFS 66V spectrometer in the range of 4000-400cm^{-1}. The spectral resolution was ± 2cm^{-1}. The FT-Raman spectra of these compounds were also recorded in the same instrument with FRA 106 Raman module equipped with Nd:YAG laser source operating at 1.064μm line widths with 200mW power. The spectra were recorded in the range of 3500-100cm^{-1} with scanning speed of 30cm^{-1}min^{-1} of spectral width 2cm^{-1}. The frequencies of all sharp bands were accurate to ± 20cm^{-1}. The UV-Vis absorption spectrum of the sample was examined in the range of 200-400nm using Shimadzu UV-1800 PC, UV-Vis recording spectrophotometer.

3. Computational details

To provide complete information regarding the structural characteristics and the fundamental vibrational modes of CFX, the B3LYP correlation functional calculations were carried out. The calculations of geometrical parameters in the ground state were performed using the Gaussian 03[10] program. DFT calculations were carried out with Becke's three-parameter hybrid model using the Lee-Yang-Parr correlation functional (B3LYP) method. The optimized structural parameters were used in the vibrational frequency calculations at DFT level to characterize all stationary points as minima. The optimized structural parameters were evaluated for the calculations of vibrational frequencies by assuming C1 point group symmetry. The assignments of the calculated wavenumbers were aided by the animation option of Gauss View 5.0 graphical interface from Gaussian program [11]. As a result, the unscaled calculated frequencies, reduced mass, force constants, infrared intensities, Raman activities and depolarization ratio were obtained. The symmetry of the molecule was also helpful in making vibrational assignments. The symmetries of the vibrational modes were determined by using the standard procedure [12] of decomposing the

traces of the symmetry operation into the irreducible representations. The symmetry analysis for the vibrational modes of CFX was presented in detail in order to describe the basis for the assignments. By combining the result of the Gauss View program [13] with symmetry considerations, vibrational frequency assignments were made with a high degree of confidence. There is always some ambiguity in designing internal coordinates. However, the defined coordinates form complete set and matches quite well with the motions observed using the Gauss View program. UV-Vis spectra, electronic transitions, vertical excitation energies and absorbance were computed with the time-dependent DFT (TD-DFT) method. The electronic properties such as HOMO and LUMO energies were determined by TD-DFT approach.

4. Results and discussion

4.1 Geometric Structure

The optimized molecular structure of CFX belongs to C_1 point group symmetry. The most optimized geometry performed at B3LYP/6-31G(d,p) basis set of CFX molecule with atom numbering scheme is shown in Fig.1. The comparative optimized structural parameters such as bond length, bond angle are presented in Table 1. The theoretical values for the CFX molecule were compared with the experimental values by means of the root mean square deviation values [14]. The C_{14}-$C1_5$ bonds were found to be shorter than the other bonds of CFX. This molecule has seven N-C bond lengths, twelve C-C bond lengths, one C-S bond length, thirteen C-H bond lengths, four C-O bond lengths, one O-H bond length, one C-Cl bond length, two N-H bond length. The O_{11}-H_{29} bond length value was found to be 0.9889Å. Here the value of C_4-S_5 bond length was found to be high compared to other bond length values. Several researchers have explained the changes in the frequency or bond length or bond angle of the C-H bond on substitution due to change in the charge distribution on the carbon atom of the ring. The calculated bond angle of C_2-N_1-C_8 is 134.51° is found to be high compared to other values of bond angle. The small difference between experimental and theoretical bond lengths and bond angles may be due to the presence of intermolecular hydrogen bonding.

4.2 Vibrational analysis

The title molecule CFX has 41 atoms, belonging to C1 point group and possessing 104 normal vibrational modes. The vibrational spectral assignments were performed based on the recorded FT-IR and FT-Raman spectra and the theoretically predicted wavenumbers of the title molecule. Vibrational frequencies of CFX were calculated by B3LYP with basis set 6-31G(d,p) level. The observed peaks were compared with the calculated results to facilitate the assignments of the peaks and are tabulated in Table 2. The experimental and theoretical FT-IR and FT-Raman spectra of CFX are shown in Figs.2 and 3. The theoretically simulated spectra are more regular than the experimental ones because many vibrations presenting in condensed phase lead to strong perturbation of infrared and Raman intensities of many other modes. Fogarsi and Pulay et al. recommended the natural internal coordinates [15,16]. The calculated harmonic wavenumbers are usually higher that the corresponding experimental quantities because of the combination of electron correlation effects and the basis set deficiencies. The maximum number of values determined by B3LYP/6-31G(d,p) is in good agreement with the experimental values.

4.2.1 CH_3 Vibrations

Methyl groups are generally referred to as electron donating substituent's in the aromatic ring system. The C-H stretching in CH_3 occurs at lower frequencies than those of aromatic ring. For CH_3 compound, the modes appearing in the region 2962 – 2872 cm^{-1} are assigned to CH_3 stretching mode of vibration [17,18]. In the present work, the FT-IR bands observed at 2931, 2919 and 2905 cm^{-1} and the FT-Raman bands observed at 2930, 2918 and 2905 cm^{-1} have been assigned to CH_3 stretching vibrations [19-21]. The B3LYP level at 6-31G(d,p) basis set values are 2930, 2919 and 2904 cm^{-1} as shown in Table 2. In general, the aromatic CH_3 stretching vibration calculated values are in good agreement with the experimental values. These vibrations are identified as pure mode with 100% of PED values.

4.2.2 C-H Vibrations

Aromatic compounds commonly exhibit multiple weak bands in the region 3200 – 3000 cm^{-1} due to aromatic C-H stretching vibrations [22-25]. The C-H symmetric stretching vibrations observed in FT-IR spectrum at 3091 cm^{-1} , similarly in FT-Raman spectrum at 3088 cm^{-1}. The C-H in-plane and out-of-plane bending vibrations generally lie in the range 1300-1000 cm^{-1} and 950-800 cm^{-1} respectively [26,27]. The calculated values of these modes for the title molecule have been found to be 3090 cm^{-1} at B3LYP level with 6-31G(d,p) basis set calculation. As indicated by the PED, these modes involve approximately 100% contribution suggesting that they are stretching modes. The substituted benzene like molecule gives rise to C-H stretching, C-H in-plane and C-H out-of-plane bending. The in-plane C-H bending vibrations appear in the range 1475-1450 cm^{-1} [28] in the substituted benzenes and the out-of-plane bending vibrations occur in the frequency range 750-1000 cm^{-1}[29]. The calculated frequencies are 964, 939 and 829 cm^{-1} assigned to C-H torsion bending vibrations for CFX. This also shows good agreement with the experimental values as given in Table 2.

4.2.3 C-N Vibration

The identification of C-N vibration is a very difficult task, since the mixing of several bands is possible in this region. The C-N stretching vibrations generally occur in the region 1180-1280 cm^{-1}[28]. James et al. [30] assigned 1370 cm^{-1} for 1-benzyl-1-H-imidazone for C-N vibration. Pinchaset et al. [31] assigned C-N stretching at 1368 cm^{-1} in benzamide. Kahorec and Kohlrensch et al. [32] identified the stretching wavenumber of C-N band in Salicylcaldoxinne at 1617 cm^{-1}. In the present investigation the bands observed at 1489 and 1330 cm^{-1} in FT-IR and 1489, 1360 and 1331 cm^{-1} in FT-Raman are assigned to C-N stretching vibration as given in Table 2. The theoretically calculated value of C-N stretching vibrations are 1489 and 1330 cm^{-1} by B3LYP level with 6-31G(d,p) basis set.

4.2.4 C-O vibrations

The C-O stretching vibration in CFX has a main contribution in the mode with B3LYP/6-31G(d,p) predicted frequency at 1749 cm^{-1}. In the present investigation the bands were observed at 1717 cm^{-1} and at 1717 cm^{-1} in FTIR and FT-Raman spectrum of CFX respectively. The C-O bending vibration mode with the experimental frequency of 1717 cm^{-1} was found to be in excellent agreement with the calculated value at B3LYP level.The conclusions above are in agreement with the literature value [33].

4.2.5 N-H Vibrations

It has been observed that the presence of N-H group in various molecules may be correlated with a constant occurrence of absorption bands whose positions are slightly altered from one compound to another; this is because the atomic group vibrates independently of the other groups in the molecule and has its own frequency. The intensity of absorption in this region depends upon the degree of hydrogen bonding, and hence upon the physical state of the sample. Normally in all the heterocyclic compounds, the N-H stretching vibration occurs in the region of 3500-3000 cm^{-1}[34]. In our title molecule, the N-H stretching vibration, is predicted at 3481 cm^{-1} by B3LYP/6-31G(d,p) and is in very good agreement with experimental methods. This mode is pure stretching mode as it is evident from Table 2, which is exactly contributing to 100% of PED. This predicted wavenumber exactly correlate with the literature data[35].

4.2.6 C-S Vibration

In general, the assignment of the band due to C-S stretching vibrations in different compounds is difficult.The identification of C-S vibration becomes a very difficult task because of the mixing of several bands. The stretching vibrations assigned to the C-S linkage assigned to occur in the region 700-600 cm^{-1}[36]. The band observed at 599 cm^{-1} in FT-IR and 596 cm^{-1} in FT-Raman are assigned to C-S stretching mode of vibration [37]. The PED for this mode suggests that this is pure mode. The calculated wavenumber are 596 cm^{-1} by B3LYP level with 6-31G(d,p) basis set. The calculated wavenumbers are in good agreement with the experimental data and the values are in good agreement with the experimental values, as presented in Table 2.

4.2.7 C-C Vibrations

The benzene possesses six stretching vibrations of which the four with the highest wavenumbers occurring near 1650 – 1400 cm^{-1} are good group vibrations [38]. With heavy substituents, the bonds tend to shift to somewhat lower wavenumbers and greater the number of substituents on the ring, broader the absorption regions. In the title molecule, the bands observed in FT-IR and FT-Raman at 1580 cm^{-1} have been assigned to C-C stretching due to the substituents in benzene ring. The calculated C-C stretching vibrations using B3LYP/6-31G(d,p) shows a very good agreement with the experimental values.

4.2.8 NH_2 Vibrations

Primary aliphatic amides absorb in the region 3520-3320 cm^{-1} [39]. The position of absorption in this region depends upon the degree of hydrogen bonding and the physical state of the sample or the polarity of the solvent. The NH_2 stretching modes are 3462 and 3368 cm^{-1} by B3LYP level 6-31G(d,p) basis set, while the experimental values are 3368 and 3369 cm^{-1} in FT-IR and FT-Raman spectrum respectively, as presented in Table 2. The PED contributions are 100% for stretching mode.

5. Other Molecular Properties

5.1 NBO analysis

NBO(Natural Bond Orbital) analysis provides an efficient method for studying intra and inter molecular bonding and interaction among bonds, and also provides a convenient basis for investigation charge transfer or conjugations in molecular system. Another useful aspect of NBO method is that it gives information about interactions in both filled and virtual orbital spaces that could enhance the analysis of intra and intermolecular interactions. The second order Fock matrix was carried out to evaluate the donor-acceptor interactions in the NBO analysis [40]. For each donor NBO(i) and acceptor NBO(j), the stabilization energy associated with $i \rightarrow j$ delocalization can be estimated as where q_i is the donor orbital occupancy, ε_i and ε_j are the diagonal elements and F (i, j) is the off-diagonal NBO Fock matrix element. In Table 4, the perturbation energies of significant donor-acceptor interactions are presented. The larger the E(2) value, more intensive is the interaction between electron donors and electron acceptors. In CFX, the interactions between the first lone pair of nitrogen N_{17} and the antibonding of C_{14}-O_{16} have the highest E(2) value around 56.26 kcal.mol.

5.2 Molecular electrostatic potential

Molecular electrostatic potential and electrostatic potential are useful quantities to illustrate the charge distributions of molecules and used to visualize variably charged regions of a molecule. Therefore, the charge distributions can give information about how the molecules interact with another molecule. Molecular electrostatic potential regions for the electrophilic attack of charged point-like reagents on organic molecules [42]. The molecular electrostatic potential V(r) that is created in the space around a molecule by its nuclei and electrons is well established as a guide to molecular reactive behaviour. It is defined by:

in which Z_A is the charge of nucleus A, located at R_A, $\rho(r')$ is the electronic density function for the molecule and r' is the dummy integration variable [43]. At any given point r(x, y, z) in the vicinity of a molecule, the molecular electrostatic potential (MEP), V(r) is defined in terms of the interaction energy between the electrical charge generated from the molecule electrons and nuclei and a positive test charge (a proton) located at r [44]. The molecular electrostatic potential is related to electron density and a very useful descriptor for determining sites for electrophilic attack and nucleophilic reactions as well as hydrogen-bonding interactions [45,46]. To predict reactive sites for electrophilic and nucleophilic attack the investigated molecule, the MEP at the B3LYP/6-31G(d,p) optimized geometry was calculated. The different values of the electrostatic potential at the surface are represented by different colors. Potential increases in the order red<orange<yellow<green<blue. Therefore, red indicates negative regions, blue indicates positive regions, as green appears over zero electrostatic potential regions. It is accepted that the negative (red) and the positive (blue) potential regions in the mapped MESP represents regions susceptible to approach electrophilic molecules or nucleophilic molecules respectively.

In fact, the mapped MESP over a single surface does not suffice to point out which ligand's regions are more prone to oncoming electrophilic species. To really find out these regions, one should analyze MESP's contour map of the ligand .Spatial regions denser in MESP's contour lines present stronger electrostatic then region with less contour lines.Also ,electrostatic field planar projection points orthogonally towards decreasing MESP contours.Therefore, in general, the red regions depictured in the total electron density surface mapped with the MESP indicate the occurrence of inward electrostatic fields, which favor the approach of electrophilic species and repel nucleophilic ones. It can be seen that the most possible sites for electrophilic attack is C8. Negative regions in the studied molecule are found around O10,O11 and O12 atoms indicating a possible site for nucleophilic attack. According to these calculated results, the MEP map shows that the negative potential sites are on electronegative atoms as the positive sites are around the hydrogen atoms. The contour map provides a simple way to predict how different geometries can interact and is shown in Fig.4

5.3 UV-Vis spectral analysis

In an attempt to understand the nature of electronic transitions, positions of experimental absorption peaks, calculated absorption peaks(λ_{max}), vertical excitation energies(E) and assignments of the transitions of the CFX molecule were calculated and the results are presented in Table 5. The UV-Visible absorption spectra of the title compound is shown in fig.5 The electronic absorption spectra were calculated using the TD-DFT method based on the B3LYP/6-31G(d,p) level optimized structure in gas phase and water. For TD-DFT calculations, the theoretical absorption bands are predicted at 314.13, 285.82 and 283.52 nm in gas phase and 3.9105,4.2685 and 4.3349 nm in water solution. The TD-DFT calculations on electronic absorption spectra in water solvent were performed. The absorption wavelength calculated at 320 nm is in good agreement with the experimental absorption wavelength at 320 nm in the UV-Visible spectra [47-49]. The highest occupied molecular orbitals (HOMOs) and the lowest-lying unoccupied molecular orbitals (LUMOs) are named as frontier molecular orbitals (FMOs). The energy gap between the HOMOs and LUMOs as the critical parameters in determining molecular electrical transport properties helps in the measure of electron conductivity. To understanding the bonding feature of the title molecule, plot of the Frontier orbitals, such as HOMO and LUMO as shown in Fig. 6.

5.4 Mulliken population analysis

The total atomic charges of CFX obtained by Mulliken population analysis by B3LYP method with 6-31G(d,p) basis set was

Volume : 4 | Issue : 10 | October 2015 • ISSN No 2277 - 8179

listed in Table.6. The atomic charges affect dipole moment, polarizability, electronic structure and what more, more a lot of properties of molecular systems. The charge distribution of the title compound shows that all the hydrogen atoms have positive charges. All the nitrogen atoms have negative charges. The carbon atoms have either positive charges or negative charges. The maximum atomic charge is obtained for C8 when compared to other atoms. From the result it is clear that the substitution of aromatic ring leads to a redistribution of electron density. The charge distribution on the molecule has an important influence on the vibrational spectra [50]. The corresponding plot of Mulliken charges obtained by B3LYP/6-31G(d,p) level is shown in Fig.7.

5.5 Global and local reactivity descriptors

The energy gap between HOMO and LUMO is a critical parameter to determine molecular electrical transport properties. By using HOMO and LUMO energy values for a molecule, the global chemical reactivity descriptors of molecules such as hardness, chemical potential, softness, electronegativity and electrophilicity index as well as local reactivity have been defined [51-55]. Softness is a property of molecule that measures the extent of chemical reactivity. It is the reciprocal of hardness. S = using Koopman's theorem for closed-shell molecules, η, μ and χ can be defined as η = μ = χ = where A and I are the ionization potential and electron affinity of the molecules respectively. The ionization energy and electron affinity can be expressed through HOMO and LUMO orbital energies as $I = -E_{HOMO}$ and $A = -E_{LUMO}$. Electron affinity refers to the capability of a ligand to accept precisely one electron from a donor. The ionization potential calculated by B3LYP/6-31G(d,p) method for CFX is 1.5431eV. Considering the chemical hardness, large HOMO–LUMO gap means a hard molecule and small HOMO–LUMO gap means a soft molecule. One can also relate the stability of the molecule to hardness, which means that the molecule with least HOMO–LUMO gap is more reactive. Recently Parr et al. [51] have also defined a new descriptor to quantify the global electrophilic power of the molecule as electrophilicity index (ω), which defines a quantitative classification of the global electrophilic nature of a molecule Parr et al. [51] have proposed electrophilicity index (ω) as a measure of energy lowering due to maximal electron flow between donor and acceptor. Their definition of electrophilicity index (ω) is as follows: ω = Using the above equations, the chemical potential, hardness and electrophilicity index have been calculated for CFX and their values are shown in Table 7. The usefulness of this new reactivity quantity has been recently demonstrated in understanding the toxicity of various pollutants in terms of their reactivity and site selectivity [56]. The calculated value of electrophilicity index describes the biological activity of CFX.

5.6 Thermodynamic properties

The statistical thermodynamics, the standard thermodynamic functions: heat capacity($C°_{pm}$), entropy($S°_{m}$) and enthalpy ($H°_{m}$) were calculated using perl script THERMO.PL [57] and are listed in Table 8 and the correlation graph is shown in fig.8. As observed from Table 8, the values of C°pm, S°m and H°m all increase with the increase of temperature from 100 to 1000K, which is attributed to the enhancement of the molecular vibration with the temperature increase. All the thermodynamic data provide helpful information that may facilitate further study on the title compound. They compute the other thermodynamic energies according to relationships of thermodynamic functions and estimate directions of chemical reactions according to the second law of thermodynamics in thermo chemical reactions according to the second law of thermodynamics in thermo chemical field.

Note: All thermodynamic calculations were done in gas phase and they could not be used in solution.

6. Conclusions

The FT-IR and FT-Raman spectra were recorded and the detailed vibrational assignment was presented for CFX for the first time. A complete vibrational investigation of the title compound were performed using FT-IR and FT-Raman spectroscopic techniques and the various modes of vibrations were explicitly assigned the results of PED analysis. The equilibrium geometries, harmonic frequencies, infrared intensities and Raman scattering activities of the molecule were determined and analyzed by B3LYP with 6-31G(d,p) basis set. The simulated FT-IR and Raman spectra of the title compound show good agreement with the observed spectra. The electronic properties were also calculated and compared with the experimental UV-Vis spectrum. The differences between the observed and the scaled wavenumbers values of most of the fundamentals are very small.It is believed that this study reveals the interesting spectroscopic and electronic properties of the title compound, which will be useful to those who are in the pursuit of experimental and theoretical details of the title molecule.

Table 1 Optimized geometrical parameters of CFX

Bond length(Å)	B3LYP 6-31G(d,p)	Bond angle(°)	B3LYP 6-31G(d,p)	Bond angle(°)	B3LYP 6-31G(d,p)
$N_1 - C_2$	1.4226	$C_{22} - H_{38}$	1.0861	$C_{20} - C_{19} - H_{35}$	120.19
$N_1 - C_6$	1.4666	$C_{23} - H_{39}$	1.0877	$C_{10} - C_{90} - C_{91}$	120.24
$N1 - C_8$	1.3794	$N_{24} - H_{40}$	1.0155	$C_{19} - C_{20} - H_{36}$	119.73
$C_2 - C_3$	1.3548	$H_{24} - H_{41}$	1.0179	$C_{21} - C_{20} - H_{36}$	120.01
$C_3 - C_6$	1.3548	$S_5 - C_4 - H_{25}$	108.9	$C_{90} - C_{91} - C_{99}$	119.7
$C_3 - C_4$	1.5203	$S_5 - C_4 - H_{26}$	104.81	$C_{20} - C_{21} - H_{37}$	120.121
$C_3 - C_{13}$	1.5076	$H_{25} - C_4 - C_6$	106.2	$C_{22} - C_{21} - H_{37}$	120.16
$C_4 - S_5$	1.8387	$C_4 - S_5 - C_6$	93.76	$C_{91} - C_{99} - C_{92}$	119.99
$C_4 - H_{25}$	1.0974	$N_1 - C_6 - S_5$	110.71	$C_{21} - C_{22} - H_{38}$	120.18
$C_4 - H_{26}$	1.0945	$N_1 - C_6 - C_7$	87.82	$C_{23} - C_{32} - H_{39}$	119.82
$S_5 - C_6$	1.8251	$N_1 - C_6 - H_{27}$	11.1908	$C_{18} - C_{99} - C_{99}$	120.68
$C_6 - C_7$	1.5693	$S_5 - C_6 - C_7$	115.58	$C_{18} - C_{23} - H_{39}$	119.56
$C_6 - H_{27}$	1.0928	$S_5 - C_6 - H2_7$	110.87	$C_{22} - C_{23} - H_{39}$	119.74
$C_7 - N_{17}$	1.4275	$C_7 - C_6 - H_{27}$	116.68	$C_{15} - N_{24} - H_{40}$	110.06
$C_7 - H_{28}$	1.0928	$C_6 - C_7 - N_{17}$	120.51	$C_{15} - N_{24} - H_{41}$	108.45
$C_8 - O_{12}$	1.2185	$C_6 - C_7 - H_{28}$	112.12	$H_{40} - N_{24} - H_{41}$	108.18
$C_9 - O_{10}$	1.3347	$N_{17} - C_7 - H_{28}$	107.48	$C_9 - N_1 - C_6$	126.11
$C_9 - O_{11}$	1.3347	$N_1 - C_8 - O_{12}$	131.71	$C_9 - N_1 - C_8$	134.51
$O_{11} - H_{30}$	0.9889	$C_9 - C_8 - O_{10}$	121.91	$C_6 - N_1 - C_8$	94.52
$C_{13} - H_{30}$	1.0857	$C_9 - C_8 - O_{11}$	117.7	$N_1 - C_1 - C_9$	119.18
$C_{13} - H_{31}$	1.0857	$O_{10} - C_8 - O_{11}$	120.37	$N_1 - C_1 - C_9$	116.76
$C_{13} - H_{32}$	1.0973	$C_9 - O_{11} - O_{29}$	115.31	$C_{14} - N_{17} - H_{24}$	119.31
$C_{14} - C1_5$	0.5367	$C_9 - C_{13} - H_{30}$	109.78	$C_{15} - C_{19} - C_{92}$	120.6
$C_{14} - O_{16}$	1.2236	$C_9 - C_{13} - H_{31}$	112.56	$C_{10} - C_{19} - C_{92}$	120.44
$C_{14} - N_{17}$	1.3729	$C_9 - C_{13} - H_{29}$	109.55	$C_{10} - C_{19} - C_{92}$	118.942
$C_{15} - C_{18}$	1.5319	$H_{30} - C_{13} - H_{31}$	108.25	$C_{18} - C_{10} - C_{90}$	120.42
$C_{15} - N_{24}$	1.4597	$H_{30} - C_{13} - H_{32}$	106.59	$C_{18} - C_{19} - H_{35}$	120.24
$C_{15} - H_{32}$	1.0993	$H_{31} - C_{13} - H_{29}$	109.9	$C_2 - C_3 - C_6$	123.94
$N_{17} - H_{24}$	1.0099	$C_{14} - C_{14} - O_{16}$	122.11	$C_3 - C_3 - C_4$	123.78
$C_{18} - C_{10}$	1.4027	$C_{14} - C_{14} - N_{17}$	115.34	$C_3 - C_3 - C_{13}$	124.52
$C_{18} - C_{99}$	1.3988	$O_{16} - C_{14} - N_{17}$	122.5	$C_4 - C_3 - C_{13}$	111.68
$C_{10} - C_{90}$	1.3932	$C_{14} - C_{15} - N_{16}$	108.94	$C_3 - C_4 - C_5$	118.515
$C_{10} - H_{35}$	1.0862	$C_{14} - C_{15} - N_{24}$	107.31	$C_3 - C_4 - H_{35}$	108.58
$C_{99} - C_{91}$	1.3977	$C_{14} - C_{15} - H_{32}$	108.94	$C_3 - C_3 - H_{36}$	108.9
$C_{90} - H_{36}$	1.0862	$C_{16} - C_{15} - H_{24}$	115.7	$C_3 - N_{17} - C_{14}$	121.47
$C_{91} - C_{99}$	1.3943	$C_{16} - C_{15} - H_{32}$	107.48	$C_7 - N_{17} - C_{94}$	119.2
$C_{91} - H_{37}$	1.086	$N_{24} - C_{15} - H_{32}$	108.86		
$C_{99} - C_{99}$	1.3967				

Table 2 Vibrational Assignments of CFX

Mode No.	Experimental		Calculated frequency (cm^{-1})	Vibrational band assignment PED%
	frequency (cm^{-1})		B3LYP/6-31G(d,p)	
	υ(IR)	υ(Raman)	Scaled	
1	3481	3482	3481	υNH(100)
2	3462	3462	3462	$υNH_2$(63)
3	3368	3369	3368	$υNH_2$(100)
4	3333	3232	3232	υOH(99)
5	3094	3094	3094	υCH(94)
6	3090	3090	3090	υCH(98)
7	3080	3082	3081	υCH(60)
8	3072	3074	3073	υCH(63)
9	3052	3053	3052	υCH(84)
10	3007	3007	3007	υCH(98)
11	2986	2896	2986	υCH(100)
12	2986	2896	2986	υCH(59)
13	2964	2964	2964	υCH(51)
14	2931	2930	2930	$υCH_3$(81)
15	2919	2918	2919	$υCH_3$(57)
16	2905	2905	2904	$υCH_3$(100)
17	1766	1767	1767	$υOC_2$(48)
18	1750	1749	1749	$υOC_2$(83)
19	1717	1717	1718	υOC(79)
20	1580	1580	1580	υCC(86)
21	1489	1489	1489	υNC(19)+ δHNC(51)
22	1477	1477	1478	δHCC(17)
23	1456	1456	1457	δHCC(17)
24	1440	1441	1441	δHCC(26)
25	1428	1429	1428	δHCH(36)
26	1411	1410	1411	δHCH(84)
27	1375	1375	1375	δHOC(49)
28	1428	1427	1428	δHOC(36)
29	1411	1410	1411	δHCH(84)
30	1375	1375	1375	δHOC(49)
31	1360	1360	1360	δHNC(22)
32	1330	1331	1330	δHCC(45)+υNC(36)
33	1326	1327	1326	δHCC(69)
34	1313	1312	1313	τHCSC(15)
35	1303	1302	1302	δHCN(29)
36	1287	1285	1286	δCCC(68)
37	1252	1252	1253	δHCS(40)
38	1240	1242	1241	δHCC(32)
39	1213	1231	1213	υOC(15)
40	1183	1182	1182	υNC(29)
41	1213	1213	1213	υOC(15)
42	1213	1211	1212	υNC(14)
43	1183	1182	1182	υNC(29)
44	1175	1177	1176	τHCCN(20)
45	1164	1165	1165	δHCC(55)
46	1150	1150	1149	υCC(26)
47	1142	1144	1143	δHCC(18)
48	1126	1126	1126	τHCCC(58)
49	1101	1101	1101	υNC(36)
50	1095	1096	1095	υNC(30)
51	1062	1063	1063	υCC(93)
52	1042	1042	1043	υNC(59)+ υCC(20)+ δOCN(10)
53	1018	1018	1018	δHCH(51)+ δHCS(36)+ τHCCC(13)
54	1018	1017	1017	υCC(23)+ δHCC(10)
55	1011	1011	1010	υCC(10)+ υNC
56	964	964	964	τHCCC(25)
57	938	939	939	τHCCC(47)
58	930	930	930	υCC(35)
59	905	905	906	υCC+ δCNC(17)
60	895	895	895	$τHCCC_3$(46)
61	873	872	872	$τHCC_2$(24)
62	870	870	870	$υCC_3$(23)
63	844	843	844	τHCSC(27)
64	828	829	829	$τHCCC_2$(28)
65	809	808	809	τHOCC(19)
66	801	801	800	τHOCC(24)+ γOCNC(12)
67	787	789	788	υOCOC(29)
68	763	764	763	τHCCC(11)
69	730	729	729	δCCC(13)+ τHOCC(26)+υOCOC(72)
70	722	723	723	τHOCC(10)
71	691	691	691	τCCCC(52)
72	685	687	686	τCCC(69)
73	609	608	608	$δCCC_3$(35)
74	599	596	596	υSC(56)+γOCNC(42)
75	-	579	579	γNCCC(58)
76	-	540	540	δOCC(11)+τCCNC(10)
77	-	496	496	τHNCC(44)
78	-	478	479	δCCN(17)+ δSCN(13)+υCCN(10)
79	-	453	454	τHNCC(44)
80	-	446	446	τHNCC(58)+ υCC(11)
81	-	401	401	γCCCC(23)+δOCC(46)
82	-	399	400	$τCCCC_3$(51)

Volume : 4 | Issue : 10 | October 2015 • ISSN No 2277 - 8179

83	-	349	349	δCCC(44)
84	-	311	312	δNCC(10)
85	-	311	311	δNCC(17)
86	-	299	299	δNCC(11)+γCCCC(58)
87	-	284	285	δOCC+δNCC(2)+ δCCC(16)
88	-	272	272	δOCN(12)+ δCNC(12)
89	-	253	254	δCCC(19)+τHNCC(39)
90	-	241	240	δCCC(17)
91	-	201	200	δCCC(16)+ δCNC(13)+γCNCC(12)
92	-	183	183	δNCC(12)+δCNC(17)+ δCCC(69)
93	-	166	167	δNCC(34)+δCNC(17)+ δCCC(56)
94	-	160	160	γCCCC(23)+δOCC(46)
95	-	124	123	τCCNC(51)+ τCNCC(27)+γCCCN(12)
96	-	118	118	τCCCN(23)
97	-	97	98	δCCC(26)
98	-	91	92	τCCCN(53)
99	-	77	77	τOCCN(41)+ γCNCC(51)
100	-	68	68	δCNC(24)+τCCNC(58)+ τCCCN(12)
101	-	46	46	τNCCC(62)+ τCCNC(13)
102	-	39	40	δCCN(24)+τNCCN(29) +τCNCC(20)
103	-	16	17	τCNCC(43)+τCCCC(17)+ γCCCC(11)
104	-	12	10	τNCCC(47)+τCCNC(45)

υ-stretching; δ-bending; γ-Out of plane bending; τ-torsion; potential energy distribution (PED);

Table 3 IR intensity and Raman activity of CFX

S.No	$IR_{int.}$	$Ram_{act.}$	S.No	$IR_{int.}$	$Ram_{act.}$	S.No	$IR_{int.}$	$Ram_{act.}$
1	827	49.1	39	34.86	6.05	77	25.79	2.9
2	8.36	113.72	40	5.84	6.7	78	13.17	1.49
3	2.55	47.63	41	113.32	11.53	79	16.67	6.18
4	17	276.46	42	38	6.57	80	0.1	3.93
5	20.34	24.67	43	59.33	7.96	81	4.37	1.32
6	11.26	90.4	44	10.78	6.62	82	25.07	3.06
7	0.65	67.35	45	3.64	6.9	83	23.75	5.41
8	8.4	39.84	46	9.65	9.87	84	7.49	6.25
9	26.7	105.61	47	15.27	11.38	85	3.39	1.18
10	18.23	74.88	48	12.53	664	86	25.03	5.94
11	1.89	88.47	49	26.22	2.2	87	41.33	1
12	14.43	97.04	50	38.83	2.15	88	6.64	2.88
13	27.87	219.71	51	33.82	6.3	89	8.13	4.44
14	16.29	146.61	52	8.73	1.04	90	0.57	0.3
15	35.14	146.78	53	24	2.67	91	9.9	1.59
16	438.54	146.78	54	1.01	3.29	92	5.16	2.21
17	388.54	21.71	55	1.59	12.65	93	10.88	4.06
18	179.16	14.88	56	0.44	1.74	94	0.84	0.46
19	43.58	106.59	57	1.08	24.47	95	2.24	0.79
20	1.84	35.28	58	7.19	7.19	96	13.26	0.94
21	88.78	4.69	59	2.14	1.42	97	5.87	4.47
22	0.7	6.32	60	1.04	0.34	98	34.38	2.41
23	398.81	3.18	61	13.2	10.62	99	24.71	1.9
24	39.71	0.7737	62	5.24	3.97	100	19.46	0.19
25	13.46	16.18	63	4.95	0.42	101	3.26	1.44
26	7.48	0.9	64	147.94	2.2	102	0.66	2.23
27	22.34	55.43	65	13.78	1.19	103	0.4	2.81
28	9.38	23.65	66	0.97	1.57	104	3.52	2.25
29	396.08	13.62	67	0.52	4.42	105	2.53	0.19
30	26.39	27.6	68	36.93	10.05	106	5.3	3.22
31	9.44	6.83	69	89.53	2.8	107	0.14	0.77
32	18.24	15011	70	8.25	1.75	108	0.39	0.68
33	45.26	12.85	71	6.18	4.54	109	0.33	2.23
34	1.04	0.35	72	8.09	2.49	110	3.32	2.39
35	110.85	27.88	73	33.87	3.53	111	0.21	0.37
36	13.57	11.9	74	8.28	1.94	112	0.44	7.12
37	32.75	13.07	75	39.21	6.05	113	0	4.57
38	1.88	2.85	76	18.65	2.88	114	0.25	1.8

Table 4 Second order perturbation theory analysis of Fock matrix in NBO analysis

Donor(i)	Acceptor(j)	E(2)[a] (kJ/mol)	E (j) – E (i) [b] (a.u.)	F(i, j)[c] (a.u.)
π C_{16}-C_{19}	π * C_{20}–C_{21}	19.53	0.27	**0.065**
π C_{20}–C_{21}	π * C_{22}–C_{23}	20.43	27	**0.066**
π C_{20}–C_{22}	π * C_{16}–C_{19}	20.48	0.27	0.067
LP_1 – N_1	π * C_8–O_{12}	20.98	0.37	0.08
LP_2 – O_{10}	π * C_7–C_8	20.1	0.63	0.102
LP_2 – O_{10}	π * C_8–O_{11}	31.08	0.63	0.117
LP_2 – O_{12}	π * N_1–C_8	27.5	0.5	0.116
LP_2 – O_{12}	π * C_7–C_8	36.32	0.41	0.111
LP_2 – O_{16}	π * C_{14}–C_{15}	22.4	0.64	0.109
LP_2 – O_{16}	π * C_{14}–C_{17}	27.83	0.71	0.127
LP_3 – N_{17}	π * C_{14}–O_{16}	56.26	0.29	**0.116**

[a] E(2) means energy of hyper conjugative interaction (stabilization energy).

[b] Energy difference between donor and acceptor i and j NBO orbitals.

[c] F(i,j) is the fock matrix element between i and j NBO orbitals.

Table 5 UV-Vis excitation energy(ΔE) of CFX

States	TD-B3LYP/6-31G(d,p)				Expt. λ
	Gas phase		Water		
	λcal	E(eV)	λcal	E(eV)	
S1	314.1300	3.9468	3.9105	0.0227	**320**
S2	285.82	4.3379	4.2685	0.0115	**280**
S3	283.52	4.373	4.3349	0.0005	**269**

Table 6 Mulliken atomic charges of CFX

Atoms	B3LYP 6-31G(d,p)	Atoms	B3LYP 6-31G(d,p)	Atoms	B3LYP 6-31G(d,p)	Atoms	B3LYP 6-31G(d,p)
N1	-0.446283	O11	-0.474173	C21	-0.086124	H31	0.15692
C2	0.178918	O12	-0.423042	C22	-0.094647	H32	0.123572
C3	0.072037	C13	-0.375066	C23	-0.115719	H33	0.124455
C4	-0.397883	C14	0.579705	N24	-0.55713	H34	0.303647
S5	0.139885	C15	0.087607	H25	0.140334	H35	0.119075
C6	-0.136666	O16	-0.48545	H26	0.149963	H36	0.094066
C7	0.013115	N17	-0.535692	H27	0.175996	H37	0.089724
C8	0.534204	C18	0.075373	H28	0.152461	H38	0.092065
C9	0.486139	C19	-0.110449	H29	0.336394	H39	0.080374
O10	-0.397387	C20	-0.10623	H30	0.132347	H40	0.233504
						H41	0.245272

Table 7 Molecular properties of CFX

Molecular properties	B3LYP/6-31G(d,p)	Molecular properties	B3LYP/6-31G(d,p)
εHOMO(eV)	6.4597	Chemical hardness(η)	-6.4597
εLUMO(eV)	-1.5431	Chemical potential(μ)	-0.2499
ε(H-L) (eV)	4.7166	Electronegativity(χ)	2.4583
Ionization potential(I)	1.5431	Electrophilicity index(ω)	3.0216
Electron affinity(A)	-4.0014	Softness(S)	-2.4583

Table 8 Thermodynamic functions of CFX

Temperature (T°K)	Entropy (J/mol.K)	Enthalpy (J/mol.K)	Heat Capacity(KJ/mol)
100.00	434.76	162.00	10.34
200.00	579.08	266.48	31.76
298.15	705.13	371.93	63.09
300.00	707.44	373.89	63.78
400.00	828.99	473.55	106.27
500.00	943.90	556.55	157.92
600.00	1051.48	623.05	217.03
700.00	1151.67	676.41	282.09
800.00	1244.93	719.88	351.98

900.00	1331.86	755.85	425.82
1000.00	1413.10	785.97	502.95

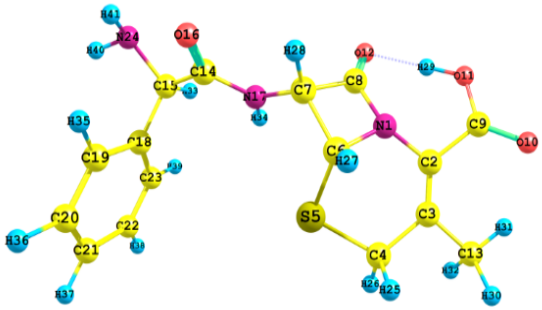

Fig.1 Optimized Structure of CFX

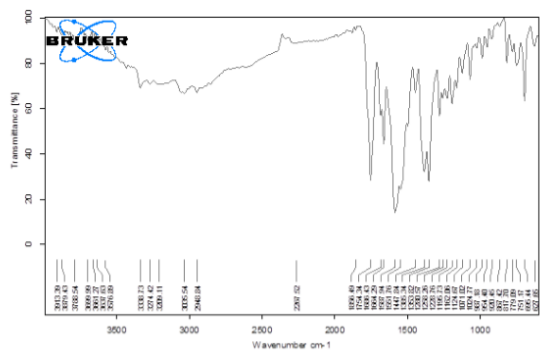

Fig.2 Experimental FT-IR spectra of CFX

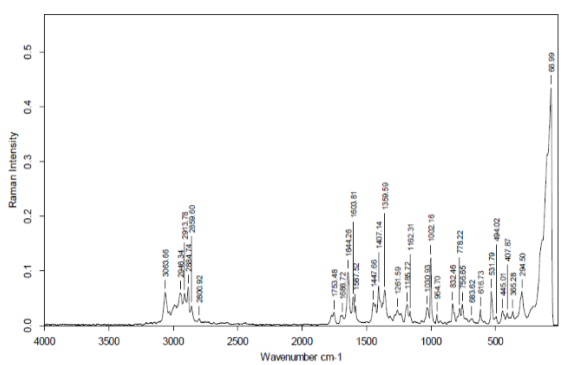

Fig.3 Experimental FT-Raman spectra of CFX

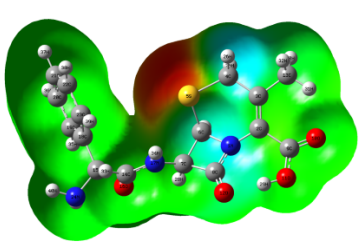

Fig. 4 Molecular electrostatic potential of CFX

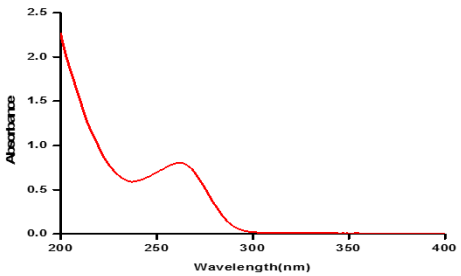

Fig.5 UV-Visible spectrum of CFX

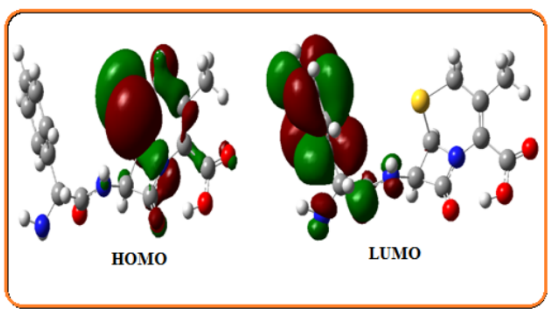

Fig. 6 Frontier molecular orbital of CFX

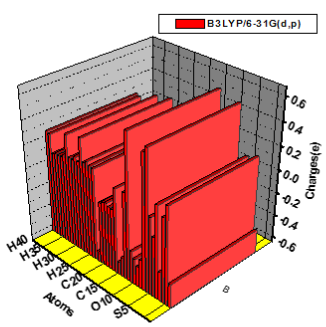

Fig. 7 Mulliken atomic charges of CFX

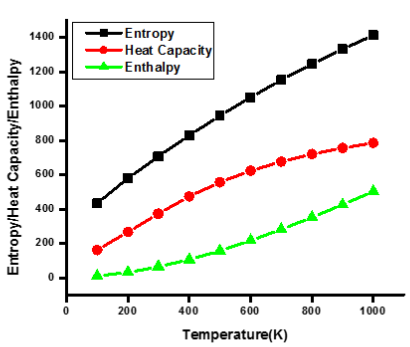

Fig.8 Thermodynamic properties of CFX

REFERENCE

[1] K.J.Madaras-Kelly, R.E.Remington, C.M.Oliphant, et.al, Efficiacy of oral τ-lactam treatment of ulcompicated cellulitis, AMJ.Med.,(2008), 121, 417-425. [2] B.A.Cunha, Oral antibiotic therapy of serious systematic infections, Med.Clin.North.Am.(2006) 90, 1197-1222. [3] B.A. Cunha, Intravenous to oral antibiotic switch therapy, Drugs Today(Barcelona), (2001), 37, 311-319. [4] P.White, Surface enhanced resonance scattering spectroscopy, In J.Robertson, M.Grive, editors Forensic examination of fibers, 2nd edt. New York, Taylor and Francis Group, (1999), 337-342. [5] R.S.Golightly, W.E.Doering, M.J.Natan, Surface enhanced and homeland security, a perfect match ACS Nano, (2009), 10, 2859-2869. [6] D.J.W.Grant, Theory and origin of polymorphism, In; H.G.Brittain, ed. Polymorphism in pharmaceutical solids, Newyork; marcel Dekker, (2000), 1-33. [7] L.Yu, Amorphous pharmaceutical solids; Preparation Characterization and stabilization, Adv.Drug.Deiv.Rev, (2001), 48, 27-42. [8] D.Giron, et.al, Solid-State of pharmaceutical compounds-impact of the KHQ6 guideline on industrial development J.Therm.Anal.Cal, (2004), 77, 709-747. [9] A.H.Kuptsov, Applications of Fourier Transform Raman spectroscopy in Forensic Science, J.Forensic Sci, (1994), 39, 305-318. [10] Gaussian 03 program, Gaussian Inc., Wallingford CT, 2004. [11] A. Frisch, A.B. Nielson, A.J. Holder, GAUSSVIEW User Manual, Gaussian Inc., Pittsburgh, PA, 2000. [12] F.A.Cotton, Chemical Applications of Group Theory, Wiley Interscience, New York 1971. [13] C.Herrmann, M.Reiher, Top.Curr.Chem, 268 (2007) 85-132. [14] P.Pulay, in:H.F.Schalfer III(Ed), Applications of Electronic Structure Theory, Modern Theoretical Chemistry, Vol.4.Plenum, NewYork, 1997, p.p.153. [15] P.Pulay, X.Zohu, G.Fogarsi, in: R.Fransto(Ed), NATO ASI Series, 406, Kluwer, Dordrecht, 1933, p.p.99. [16] M.Silverstein, G.Clayton Basseler, C.Morill, Spectrometric Identification of Organic compounds, Wiley, NewYork, 1981. [17] G.Socrates, Infrared Characteristic Group frequencies, Wiley-Interscience Publication, NewYork, 1980. [18] S.George, Infrared and Raman Characteristic Group Wavenumbers, Tables and Charts, third ed., Wiley, Chichester, 2001. [19] D.Lin-Vien, N.B.Clothup, W.G.Fateley, J.G.Graselli, The Hand Book of Infrared and Raman Characteristic Frequencies of Organic Molecules, Academic Press, New York, 1991. [20] G.Varsanyi, Assignments of Vibrational spectra of 700 Benzene Derivatives, Wiley, NewYork, 1980. [21] T.Gnanasambandan, S.Gunasekaran, S.Seshadri, Spectrochimica Acta A,112(2013) 52-61. [22] N.Puviarasan, V.Arjunan, S.Mohan, Turk.J.Chem, 26(2002) 323-334. [23] G.Varsanyi, Vibrational spectra of Benzene Derivatives, Academic Press, New York, 1969. [24] V.Krishnakumar, R.John Xavier, Indian.J.Pure Appl.Phys. 41(2003) 597-602. [25] V.Krishnakumar, V.N.Prabavathi, Spectrochim.Acta A 71(2008) 449-457. [26] A.Altun, K.Golcuk, M.Kumru, J.Mol.Struct. 637 (2003) 155-169. [27] M. Silverstein, G. Clayton Basseler, C. Morill, Spectrometric Identification of Organic Compounds, Wiley, New York, 1981. [28] G.Socrates, Infrared Characteristic Group frequencies, Wiley-Interscience Publication, NewYork, 1981. [29] C.James,C.Ravikumar, V.S.Jayakumar, I.HuberJoe, J.Raman Spectrosc. 40(2009) 537-545. [30] S.Pinchas, D.Samuel, M.Weiss-Broday, J.Chem.Soc.(1961) 1688-1691. [31] L.Kahvec, K.W.F.Kohlreusch, Monatsh.Chem. 74(1941) 333-343. [32] J.A.Abkowicz-Bienko, et.al., Theoretical infrared spectrum and revised assignment for para-nitrophenol density functional theory studies, Chem.Phys. 250 Issue 2(1999) 123-129. [33] N.Sundaraganesan, S.Ilakiamani, P.Subramani, B.D.Joshua, Spectrochim.ActA 67A(2007) 638-663. [34] B.Lambert, Introduction to Organic Spectroscopy Macmillan Publication, NewYork, 1987. [35] C.S.Hsu, Spectroscop.Lett 7(9), (1974) 439-447. [36] B.S.Yadav, I.Ali, P.Kumar, P.Yadav, Indian J.Pure Appl.Phys. 45(2007) 979-983. [37] M.Snehalatha, C.Ravikumar, I.H.Joe, N.Sekar, V.S.Jayakumar, Spectrochim.Acta A 72(2009) 654-662. [38] M.Szafram, A.Komasa, E.B.Adamska, J.Mol.Struct, 827(2007) 101-107. [39] A.E.Reed,L.ACurtiss, F.Weinhold, Chem.Rev.88(1988)899-926. [40] P.Politzer, D.G.Truhlar (Eds), Chemical Application of Atomic and Molecular Electrostatic Potentials, Plenum, NewYork, 1981. [41] P. Politzer, P.R. Laurence, K. Jayasuriya, Molecular electrostatic potentials: an effective tool for the elucidation of biochemical phenomena, in: J. McKinney (Ed.), Structure Activity Correlation in Mechanism Studies and Predictive Toxicology, Environ. Health Perspect, vol. 61, 1985, pp. 191–202. [42] P. Politzer, J.S. Murray, Theor. Chem. Acc. 108 (2002) 134–142. [43] F.J.Luque, J.M.Lopez, M.Orozco, Theor.Chem.Acc.103 (2000) 343-345. [44] N. Okulik, A.H. Jubert, Internet Electron, J. Mol. Des. 4 (2005) 17–30. [45] D.Shoba, S.Periandi, S.Boomadevi, S.Ramalingam, E.Fereyduni, SpectroChim.Acta A 118 (2014) 438-447. [46] M.Govindarajan, M.Karabacak, S.Periandy, D.Tanuja, Spectrochim.Acta A 97(2012) 231-245. [47] M.Govindarajan, M.Karabacak, Spectrochim.Acta A 101(2013) 314-324. [48] R.S. Mulliken, J. Chem. Phys. 23 (1995) 1833–1840. [49] R.G. Parr, L. Szentpaly, S. Liu, J. Am. Chem. Soc. 121 (1999) 1922–1924. [50] P.K. Chattaraj, B. Maiti, U. Sarkar, J. Phys. Chem. A107 (2003) 4973–4975. [51] R.G. Parr, R.A. Donnelly, M. Levy, W.E. Palke, J. Chem. Phys. 68 (1978) 3801–3807. [52] R.G. Parr, R.G. Pearson, J. Am. Chem. Soc. 105 (1983) 7512–7516. [53] R.G. Parr, P.K. Chattraj, J. Am. Chem. Soc. 113 (1991) 1854–1855. [54] R. Parthasarathi, J. Padmanabhan, M. Elango, V. Subramanian, P. Chattaraj, Chem. Phys. Lett. 394 (2004) 225–230. [55] R. Parthasarathi, J. Padmanabhan, V. Subramanian, B. Maiti, P. Chattaraj, Curr.Sci. 86 (2004) 535–542. [56] R. Parthasarathi, J. Padmanabhan, V. Subramanian, U. Sarkar, B. Maiti, P.Chattaraj, Internet Electron. J. Mol. Des. 2 (2003) 798–813. [57] K.K.Irikura, THERMO.PERL, National Institute of Standards and Technology 2002.